Atmospheric Environment 188 (2018) 142–156

Contents lists available at ScienceDirect

Atmospheric Environment

journal homepage: www.elsevier.com/locate/atmosenv

Future changes in precipitation extremes over China projected by a regional climate model ensemble

Junhong Guo[a], Guohe Huang[b,c,*], Xiuquan Wang[d,**], Yongping Li[e], Lan Yang[a]

[a] Key Laboratory of Regional Energy and Environmental Systems Optimization, Ministry of Education, North China Electric Power University, Beijing, 102206, China
[b] Institute for Energy, Environment and Sustainable Communities, University of Regina, Regina, Saskatchewan, S4S 0A2, Canada
[c] SC Institute for Energy, Environment and Sustainability Research, North China Electric Power University, Beijing, 102206, China
[d] School of Climate Change and Adaptation, University of Prince Edward Island, Charlottetown, Prince Edward Island C1A 4P3, Canada
[e] School of Environment, Beijing Normal University, Beijing, 100875, China

ARTICLE INFO

Keywords:
Extreme precipitation indices
Regional climate model
Ensemble
China

ABSTRACT

China has experienced frequent extreme precipitation events (i.e., floods and droughts) in recent years, which have resulted in significant economic losses and irrevocable damages to human societies and natural ecosystems. How to adapt to the forthcoming and long-term changes in precipitation extremes has become the top priority of decision makers and resources managers for developing resilient communities and sustainable agroecosystems. This essentially replies on a better understanding of possible changes in the spatiotemporal characteristics of precipitation extremes from both short-term and long-term perspectives. To this end, future changes in precipitation extremes across China in response to global warming are investigated in this study through a regional climate ensemble modeling approach. Specifically, in order to reflect spatiotemporal variations and uncertainties in model physics, a perturbed-physics global climate model ensemble is used to drive the PRECIS regional climate modeling system to generate 25-km climate projections throughout the 21st century for the entire country of China. The validation results for the ensemble simulations over the historical period show that the PRECIS model performs reasonably well in reproducing the spatial patterns of observed precipitation extremes in most regions of China. The future projections of precipitation extremes suggest that there is very likely to be a continuously-increasing trend in the analyzed precipitation extreme indices (except for a slight decreasing trend in CDD). Particularly, higher rates of increase in these indices are expected to occur from the forthcoming decades to the middle of this century. The results also indicate apparent spatial variations in the projected changes of precipitation extremes. In general, absolute changes in northern regions are relatively small compared to the significant changes in southeastern regions, suggesting that more severe floods might be expected in the southeast while slight increases in precipitation in the north (especially the northwest) would lead to a relief to the droughts. However, the percentage changes are larger in north than south. Moreover, it is reported that the frequency and intensity of heavy rains across the country are projected to increase, implying that more frequent urban flooding would become a major challenge for developing resilient and sustainable communities in China. The changes in thermal (i.e., temperature) and dynamical (i.e., circulations) factors could be some physical reasons for the increase of intensity and frequency in future precipitation.

1. Introduction

Precipitation is a critical component for the hydrological cycle of earth. Global warming resulted from increased greenhouse gases in the atmosphere can cause large increase in atmospheric water vapor content and lead to changes of precipitation. The Intergovernmental Panel on Climate Change (IPCC) Fifth Assessment Report (AR5) indicates that precipitation has likely increased since 1901 over the midlatitude land areas of the Northern Hemisphere (Stocker et al., 2013). Changes in precipitation not only reflect in total or mean state, but also in extremes. Most importantly, variations and trends in extreme climate events are important and more sensitive to climate change than the mean values (Li et al., 2012), because the associated devastating consequences may have huge impacts on human society (Wang et al., 2008).

As a continental country with high vulnerability to climate change

* Corresponding author. Institute for Energy, Environment and Sustainable Communities, University of Regina, Regina, Saskatchewan, S4S 0A2, Canada.
** Corresponding author.
E-mail addresses: huang@iseis.org (G. Huang), xiuquan.wang@gmail.com (X. Wang).

https://doi.org/10.1016/j.atmosenv.2018.06.026
Received 11 December 2017; Received in revised form 4 June 2018; Accepted 17 June 2018
Available online 20 June 2018

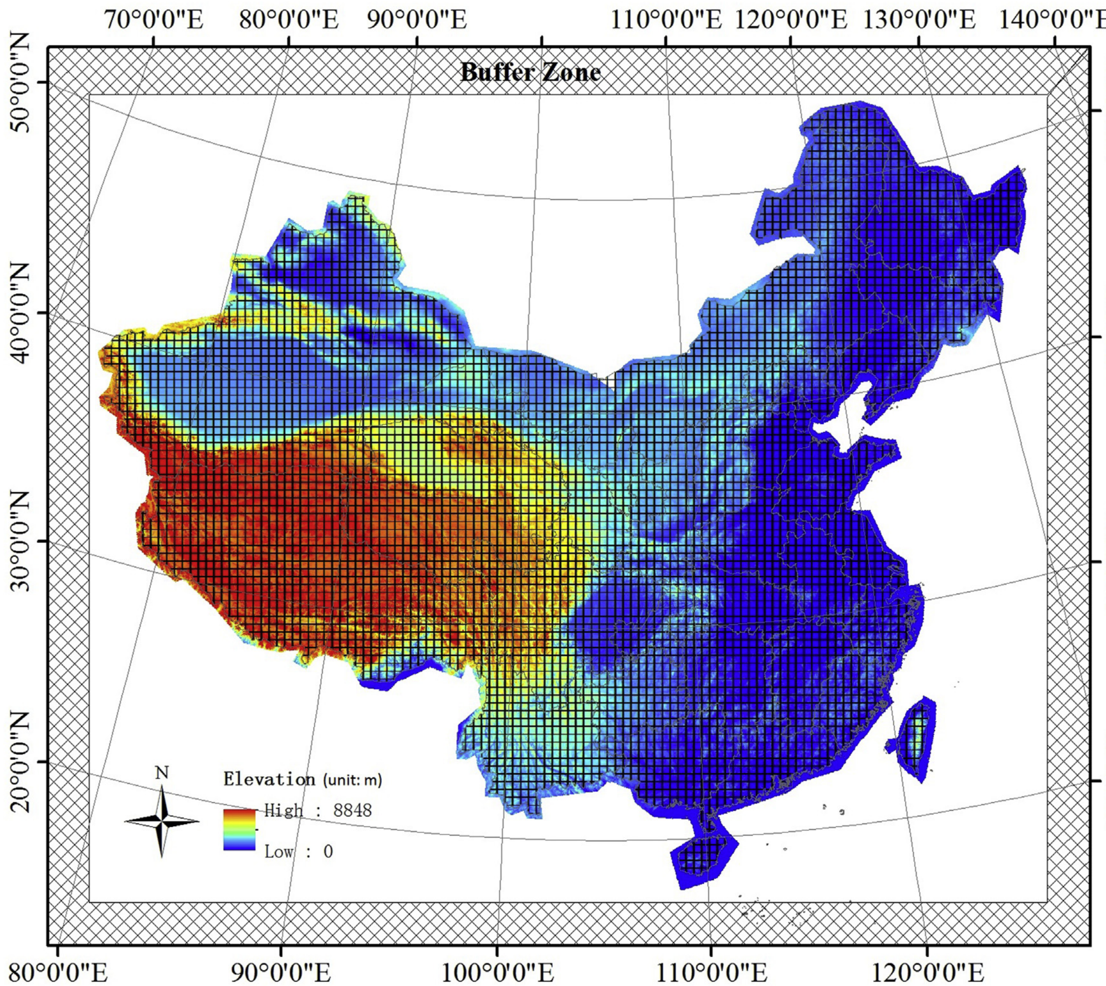

Fig. 1. Study domain. Hatched lines denote buffer zone area which is composed of 8 grids along the longitude and latitude.

and relatively low adaptive capacity, China has experienced extreme climate events and resulted in serious damage, for example, the flood of Yangtze River in 1998 (Yin and Li, 2001), freezing rain in southern China in January 2008, torrential rain and landslide in Zhouqu County of Northwest China in 2010 (Wang et al., 2012), continuous severe droughts in most parts of southern Yunnan from 2009 to 2010 (Lü et al., 2012; Qiu, 2010). These natural disasters caused hundreds of millions economic losses, large numbers of casualties and widespread displacement. To better adapt to the changing climate, the public and policy makers now urgently demand availability of reliable, long-term, and relatively high-resolution precipitation extremes information concerning future changes for developing appropriate adaptation and mitigation measures.

Nowadays, researchers have taken a great deal of effort to study precipitation extremes over China in different ways. For example, many studies are concentrated on history evaluation based on observed site datasets (Zhang et al., 2006; Fan et al., 2016). However, owing to uneven station coverage and missing values, using these data cannot reflect the reality of the entire region, especially in the remote areas or complex terrains. Another common way is that the simulated results from global coupled ocean-atmosphere circulation models (GCMs) are used to estimate the trends and variability of precipitation extremes in different emission scenarios (Zhang et al., 2006). Still, as the spatial scale of precipitation events is usually smaller than the grid sizes used by GCMs, their capabilities in projecting credible geographical distributions of future climate are often in question (Feng et al., 2011). Thus, climate model need a higher resolution for a better description of complex topography and better reproduction of small-scale atmospheric dynamics (Bell et al., 2004).

Sharing similar physical processes and mechanisms, fine-resolution regional climate models (RCMs) nested into GCMs through dynamical downscaling technologies can solve above problem well (Guo et al., 2017; Wang et al., 2012, 2016a). The outputs downscaled by RCMs with finer-scale surface forcing can produce more local or regional detail information and the results could be more credible. In this paper, we apply a dynamical downscaling modeling system (PRECIS) for climate simulations and projections over China.

The interpretation of the extreme events is not easy, because there is no single precipitation threshold indicator to represent the intensity and frequency of extremes competently. The Joint World Meteorological Organization Commission for Climatology and World Climate Research Programme project on Climate Variability and Predictability, more specifically the Expert Team on Climate Change Detection, Monitoring and Indices (ETCCDI) defined a set of climate change indices focusing on extremes that can be described from daily temperature and precipitation across different parts of the world. These indices have been widely used in detection, attribution, and projection of changes in climate extremes (Guo et al., 2017; Wang et al., 2014a; Zhou et al., 2014), in virtue of their abilities in reflecting the change of extreme climate in different aspects with relatively weak extremes, low noise and strong significances (Wang et al., 2013).

In this paper, we choose ten core precipitation extreme indices defined by the ETCCDI to portrait the characteristics of extreme precipitation. As shown in Table S1 (see supplementary materials), these

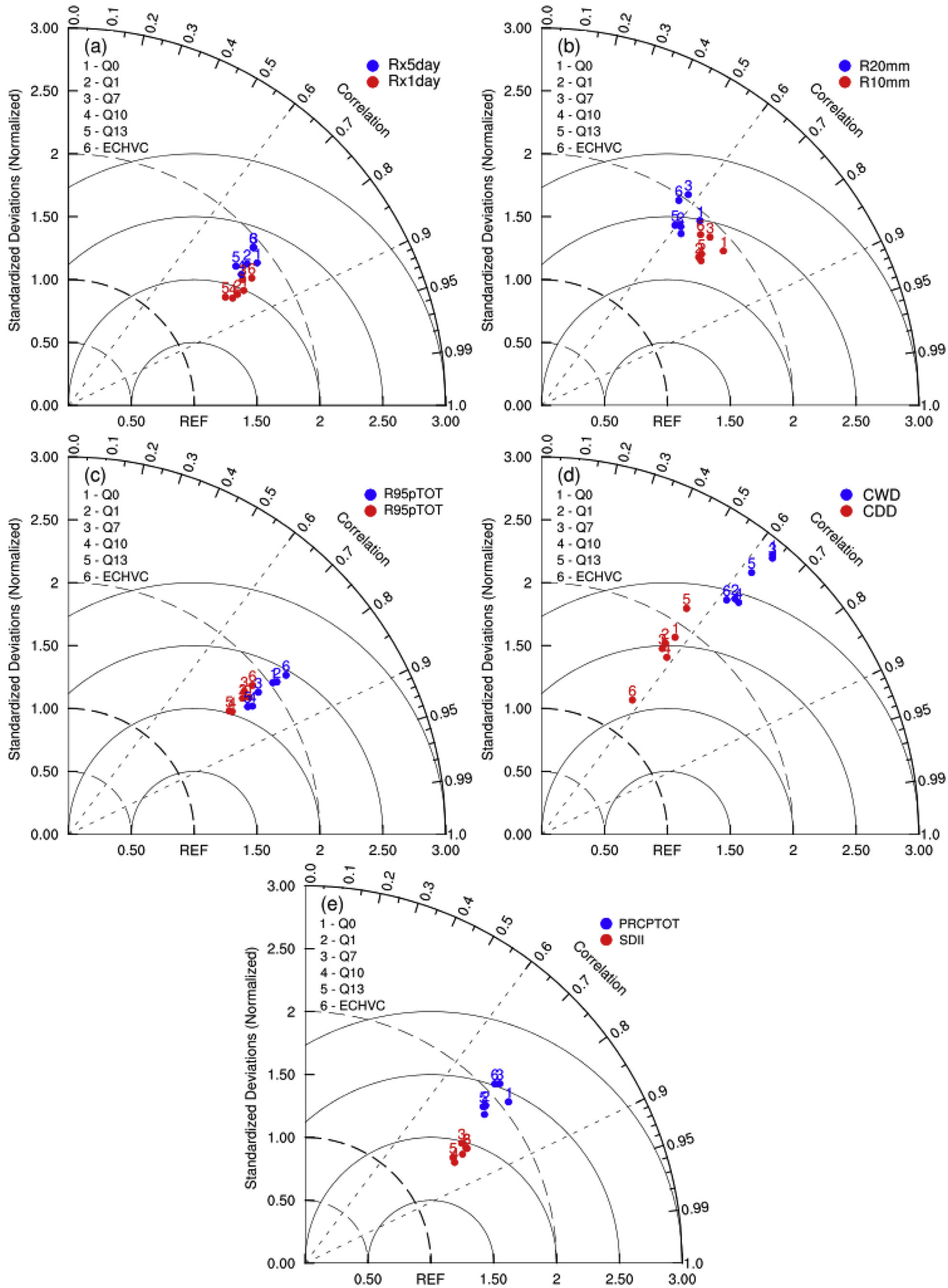

Fig. 2. Taylor diagrams of 10 indices between observation and 6 models over China. Various colors of dot represent different indices. Each dot represents a model, identified by its number on the top left. For the models located between the two blue lines, correlations are between 0.6 and 0.9. (For interpretation of the references to color in this figure legend, the reader is referred to the Web version of this article.)

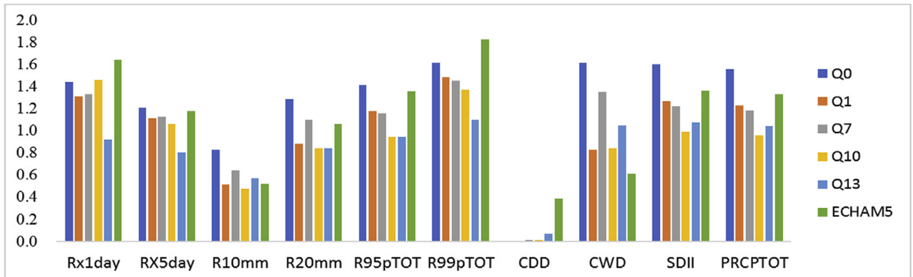

Fig. 3. Model skill scores of IVS for the 10 indices over China. The smaller IVS values, the greater the model's skill.

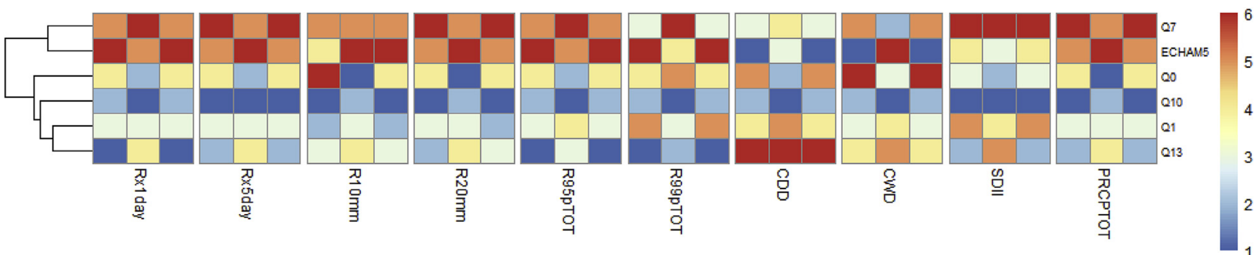

Fig. 4. The portrait diagram for the rank of each index, including correlation (left), spatial standardized deviation ratio (center), and root-mean square difference (right). Colors as marked in the label bar indicate a model's rank for each item. (For interpretation of the references to color in this figure legend, the reader is referred to the Web version of this article.)

Table 1
Weights and ranks of 6 models according to the Taylor diagram and their inter-annual variability skill (IVS) over China.

Model	Rank of Taylor	Rank of IVS	Sum of the ranks	Weights
Q0	4	6	10	0.082
Q1	3	3	6	0.137
Q7	6	4	10	0.082
Q10	1	1	2	0.411
Q13	2	2	4	0.205
ECHAM5	5	5	10	0.082

indices are classified by five categories: (1) Extremal indices, including maximum 1-day precipitation (Rx1day) and maximum 5-day precipitation (Rx5day); (2) Percentile threshold indices, including very wet day precipitation (R95pTOT) and extremely wet day precipitation (R99pTOT); (3) Absolute threshold indices, including number of heavy precipitation days (R10mm) and number of very heavy precipitation days (R20mm); (4) Spell duration indices, including consecutive dry days (CDD) and consecutive wet days (CWD); and (5) Other indices, including annual total wet-day precipitation (PRCPTOT) and simple daily intensity index (SDII). In addition, the first and second categories are regarded as the intensity of extremes and the third and the fourth represent the frequency of extremes.

As an improvement to aforementioned studies, we use the PRECIS regional climate modeling system at its highest spatial resolution (25km) to investigate the possible changes in precipitation extremes over China in response to global warming. The performance of the model is evaluated relative to an observation data set. The future changes in the spatial and temporal patterns of precipitation extremes across the country are analyzed afterwards.

2. Data and methods

2.1. Regional climate modeling

As a regional climate modeling system, the Providing Regional Climates for Impacts Studies (PRECIS) developed by the Met Office Hadley Center has been widely used to simulate climate change, because of its easy-to-use, wide suitability and flexibility (Buontempo et al., 2014; Wang et al., 2015a, 2016b). PRECIS has 50-km (0.44°) and 25-km (0.22°) resolutions at the equator of the rotated regular latitude-longitude grid and contains 19 levels in the vertical. The GCM data used to drive PRECIS is provided by the Hadley Center's global atmospheric-only model HadAM3P with a horizontal resolution of 3.75° longitude and 2.5° latitude to generate the regional model's lateral boundary conditions (LBCs). As a well encapsulated and visualized model system, the PRECIS has its unique configuration and physical parameterization schemes. For the physical parameterization schemes, the PRECIS uses a mass flux penetrative convective scheme (Gregory and Rowntree, 1990), including the direct impact of vertical convection on momentum (in addition to heat and moisture) (Gregory et al., 1997). The radiation scheme includes the seasonal and diurnal cycles of insolation, computing short wave and long wave fluxes. A first order turbulent mixing scheme is used to vertically mix the conserved thermodynamic variables and momentum (Smith, 1990). The land surface scheme is employed HadRM3P-MOSES 2.2 (Essery et al., 2001; Noguer et al., 2004). In addition, our PRECIS simulation was a continuous run from 1950 to 2099 at its implicit maximum resolution of 25 km. That means all initialization work requiring for the model to spin up and reach a stable status was carried out in the beginning years from 1950. In RCM simulations, the spin-up period is usually set to 1–2 years. Here we removed the simulations between 1950 and 1959 (10 years) in our analysis. Apparently, after these 10-year simulations, the model would certainly be able to reach a stable status. Hence, all simulations after 1960 until 2099 can be used to analyze the regional climatology for our study area.

In the climate modeling and climate change predictions, there are kinds of uncertainties, such as emission scenarios, physical feedbacks, the carbon cycle, boundary and initial conditions (Chen and Sun, 2015). These uncertainties influence our understanding towards climate change, thus none of the existed models is robust or accurate enough to guarantee the accuracy in simulation or projection, owing to different numerical implementations of climate physics. Although these uncertainties are inevitable, we can capture, quantify and further reduce them by employing multi-model ensemble to some extent (Buontempo et al., 2014; Murphy et al., 2009; Noguer et al., 2004; Wang et al., 2015b). The multi-model ensemble collects different GCM

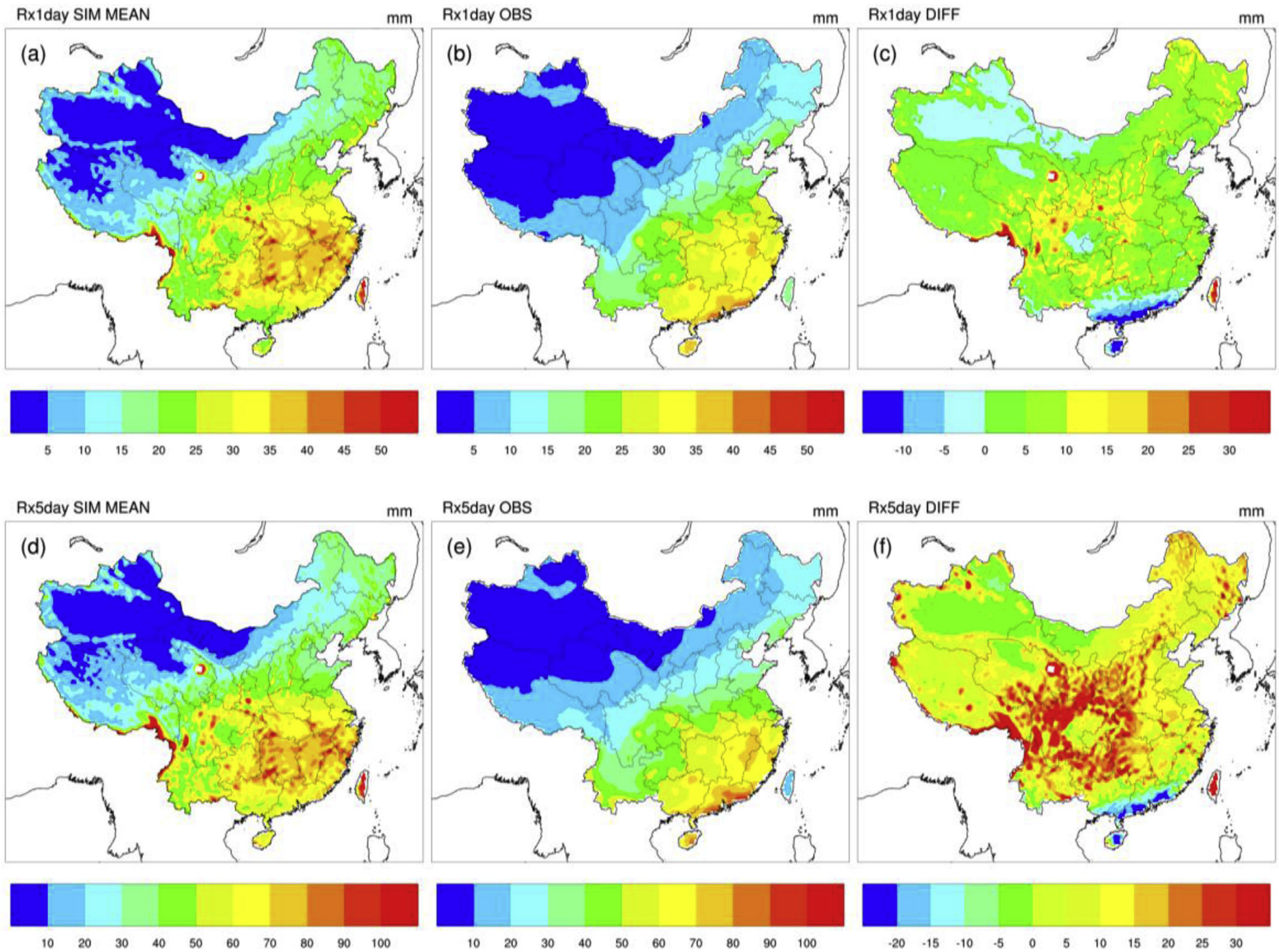

Fig. 5. Spatial comparisons (unit: mm) between simulation and observation over China for the Rx1day and Rx5day during the baseline period (1961–1990). The simulated values are the average of six simulations ensemble (Q0, Q1, Q7, Q10, Q13 and ECHAM5).

output into a central repository (i.e., CMIP3 and CMIP5) to allow inter-model comparisons and analysis (Pepler et al., 2015). Although the uncertainty range of model can be explored by this way, the disagreements between models (or external uncertainties) could be large at regional scales owing to different structural choices among models. PRECIS provides an alternative route, called "perturbed physics approach", by varying the values of the parameters in a single model to give the range of future outcomes (or internal uncertainties). Thus, the perturbations can generate larger ensembles to explore nonlinearities and extreme behavior (Collins et al., 2006; Guo et al., 2018). Specifically, the ensemble of perturbed physics LBCs in PRECIS is based on the HadCM3 model of Met Office Hadley Center for quantifying uncertainty in model projections (QUMP) under the IPCC SRES A1B emissions scenario. The QUMP ensemble consists of 17 members (HadCM3Q0-Q16) and each one has a set of perturbations to its unique dynamical and physical formulation, representing different boundary conditions and climate sensitivity (Mcsweeney et al., 2012; Wang et al., 2014b). However, considering the calculation cost and the requirements while exploring a wide range of uncertainties, we followed the suggestion from Hadley Center and selected Q0, Q1, Q7, Q10 and Q13 from the ensemble of QUMP as LBCs to run the PRECIS model. Selection of the specific ensemble members is based on 1) their performances in simulating key features of the climate over China, and 2) their ability to sample the range of outcomes of future changes simulated by the full 17-member ensemble (Bellprat et al., 2012). PRECIS will run from 1950 to 2099 with a 25-km spatial resolution, and then the time series is divided into four periods: the baseline period (1961–1990) for validation, the 2020s (2020–2040), 2050s (2041–2070) and 2080s (2071–2099) for projection. In the baseline period, we regridded the simulated results to a uniform resolution of 0.5° horizontal resolution to facilitate the comparison between observations and model simulations. The definitive China domain extends from about 66.24° E ~139.48° E and 10.07° N ~54.34° N, and covers about 38000 25-km grid points in total (Fig. 1). In addition to reflect the uncertainties associated with different parametric settings, one from ECHAM5 model, generated from the Max Plank Institute's fifth generation coupled ocean-atmosphere general circulation model, will be used to analyze the inter-model uncertainties compared with the HadCM3 downscaled by the PRECIS.

2.2. Validation methods

2.2.1. Observations

The daily precipitation observations are obtained from the gridded climate dataset CN05.1, provided by the China Meteorological Administration. Compared with other observations for China, this dataset is based on 2 416 national meteorological stations from 1961, and interpolated onto spatial grids with 0.5° × 0.5° horizontal resolution (Wu and Gao, 2013). It has been widely used in many studies of climate change across China (Ji and Kang, 2015; Wu et al., 2017). Here, we extract the data from 1961 to 1990 to represent the observations of present-day climate in the context of China.

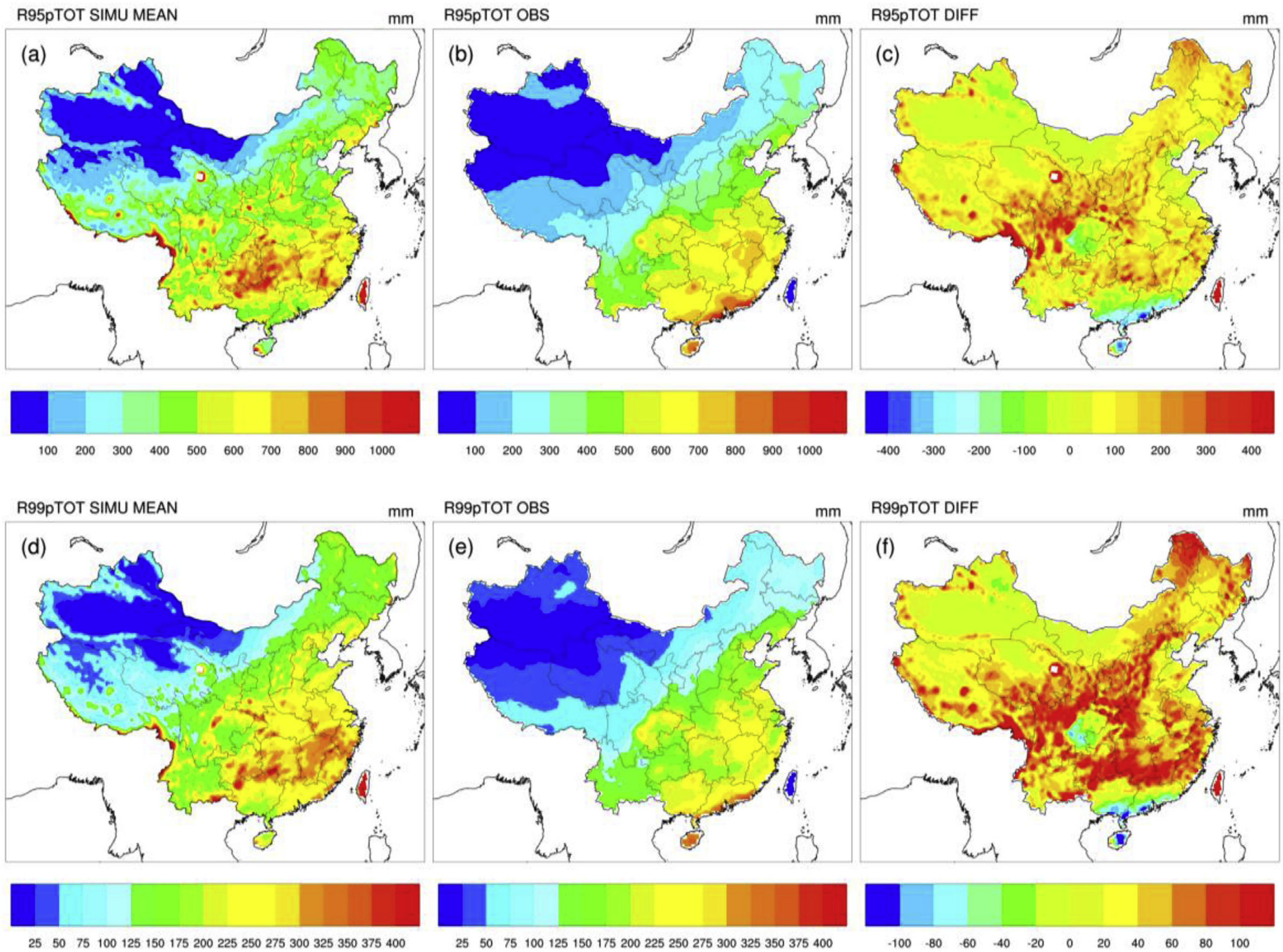

Fig. 6. Spatial comparisons (unit: mm) between simulation and observation over China for the R95pTOT and R99pTOT during the baseline period (1961–1990). The simulated values are the average of six simulations ensemble (Q0, Q1, Q7, Q10, Q13 and ECHAM5).

2.2.2. Spatial distribution

The Taylor diagram is used to test the overall performance of PRECIS in reproducing the spatial pattern of the current extreme precipitation. From the Taylor diagram, we can identify the spatial correlation coefficient, the centered pattern root-mean-square difference and the ratio of standard deviations between RCM ensemble and observation. Specifically, the spatial correlation coefficient is used to quantify the degree of phase agreement of two datasets. The centered pattern root-mean-square difference is used to measure the degree of agreement in amplitude. Normalized by the corresponding observation, if the spatial correlation and ratio of standard deviations are close to 1 and the centered pattern root-mean-square difference is close to 0, it means a good simulation (Jiang et al., 2015; Taylor, 2001).

2.2.3. Temporal variation

We apply a method called inter-annual variability skill score (IVS) to estimate the skill of PRECIS in reproducing temporal variation (Jiang et al., 2015), defined as follows:

$$IVS = \left(\frac{STD_m}{STD_o} - \frac{STD_o}{STD_m}\right)^2 \tag{1}$$

where $STD_m$and STD_o represent the inter-annual standard deviation of model simulations and observations respectively. Smaller IVS values indicate a better agreement between the simulations and observations.

2.2.4. Weight calculation

In order to comprehensively evaluate multi-model ensemble, the typical solution is to use arithmetical averaging or equal weight averaging method. Currently, many studies have applied this method for the evaluation in multi-GCMs (Chen, 2013; Chen and Frauenfeld, 2014). Nevertheless, due to the lack of individual model evaluation, equal weight among models means a high (or inferior) skillful model can be underestimated (or overestimated). In this paper, we will follow the methods mentioned by Jiang et al. (2015) and Wang et al. (2016b) to improve traditional arithmetical average. Firstly, according to Taylor diagram and IVS, ensemble models are ranked for each precipitation extreme index. Owing to three assessment indices in Taylor diagram, a comprehensive rating index MR is used to get an overall ranking, which is described as:

$$MR = 1 - \frac{1}{nm}\sum_{i=1}^{n} rank_i \tag{2}$$

Where m is the number of models, and n is the number of indices. The rank of the best-performing model is 1; the worst model is 6 for its rank. Therefore, the closer to 1 the value of MR is the higher the skill of the simulation. Secondly, we calculate the weight of each model using a function of its ranking position among others:

$$R_i = \frac{\sum_{i=1}^{n} S_i}{S_i} \tag{3}$$

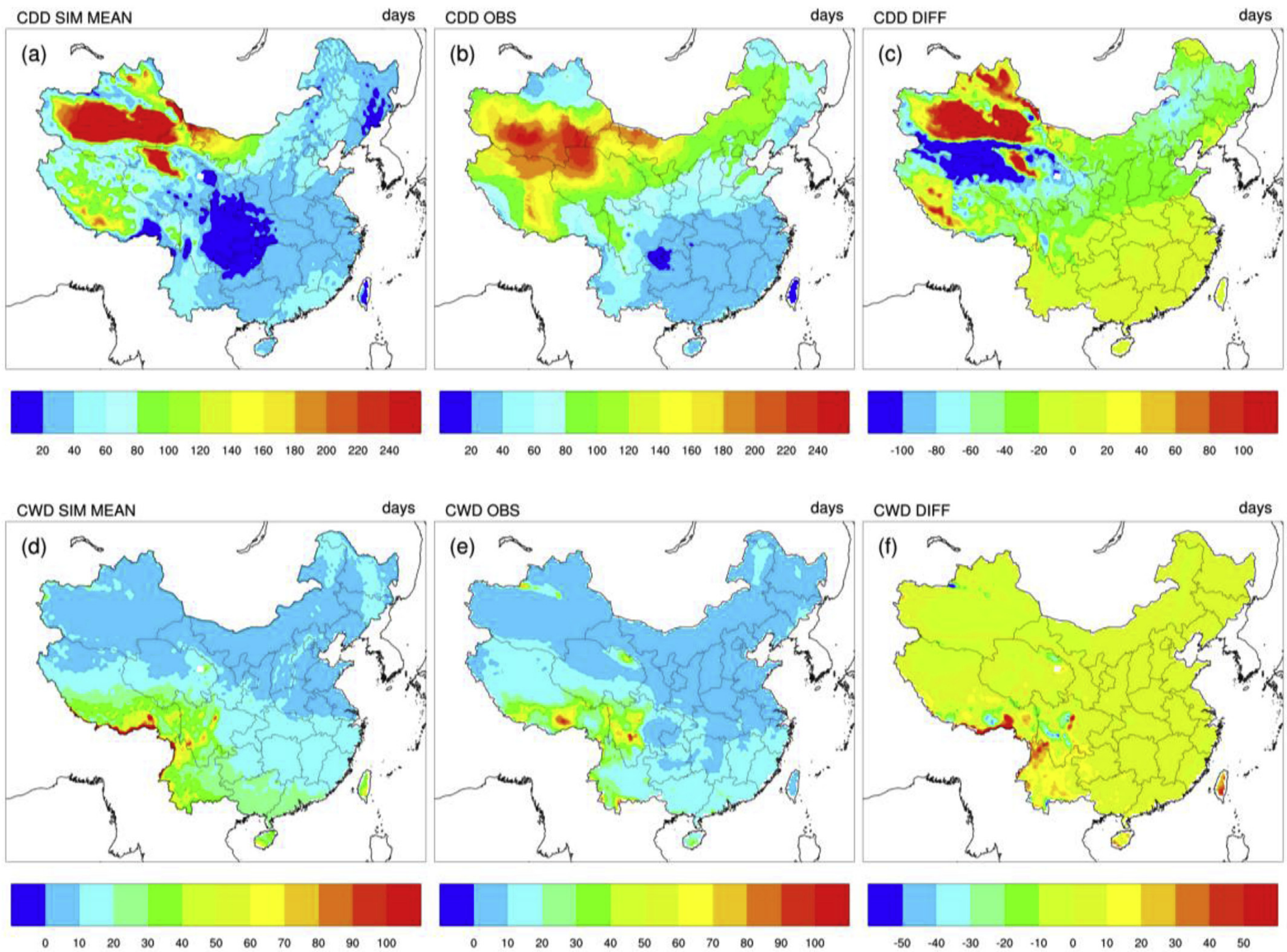

Fig. 7. Spatial comparisons (unit: days) between simulation and observation over China for the CDD and CWD during the baseline period (1961–1990). The simulated values are the average of six simulations ensemble (Q0, Q1, Q7, Q10, Q13 and ECHAM5).

$$W_i = \frac{R_i}{\sum_{i=1}^{n} R_i} \quad (4)$$

Where$S_i$is the rank of model i; $n$is the total number of models; $R_i$can be considered the combined performance indicator for an individual model; W_i is the weight of model i and it can be considered the normalized value of R_i.

2.3. Trend analyses

Trends for annual changes in future are estimated using the Mann-Kendall (MK) test. As a non-parametric statistically evaluation, MK test is often used in trend analysis on extremes, which does not assume that data are normally distributed and robustly responds to the effects of outliers in the series (Hamed and Rao, 1998; Wei et al., 2017). Additionally, the magnitude of trends will be calculated by the Theil-Sen trend estimation method, which can be more accurate than simple linear regression for statistics of skewed distribution (Fonseca et al., 2016).

3. Results

3.1. Model validation

To implement a quantitative evaluation of the performance of the six simulations in representing China's current climatologically features for ten precipitation extreme indices, we will examine their climatological spatial pattern and inter-annual variability, respectively.

3.1.1. Evaluation for spatial variation

Fig. 2 shows the Taylor diagram of the six runs against observation. For four intensity indices (Fig. 2a, c), including Rx1day, Rx5day, R95pTOT and R99pTOT, most models have high spatial correlation coefficients (0.7–0.9) and low centered pattern root-mean-square differences (1.0–1.5) with observation. In contrast, the spatial correlation coefficients of four frequency indices (R10mm, R20mm, CWD and CDD) are smaller than previous intensity indices (Fig. 2b, d), particularly for CDD with a decrease below 0.6. For CWD, the centered pattern root-mean-square difference exceeds 2.0 and the ratio of standard deviations is about 2.5, suggesting simulated amplitude of biases and variation are relative larger than observation. SDII shows the best performance among all extreme indices, with the spatial correlation coefficient of 0.85, the centered pattern root-mean-square difference of below 1.0 and the ratio of standard deviation between 1.0 and 1.5 (Fig. 2e). In addition, much larger uncertainty in frequency extremes indices than other indices are observed because of the loosely scattered distribution in the Taylor diagram, especially for consecutive dry and wet days, implying models differ widely in their simulation ability to reproduce the spatial variations for these indices. In other words, there is a large uncertainty among models when simulating the spatial pattern of frequency extremes indices in China. However, in summary, PRECIS has a reasonable performance in simulating the spatial distribution for most indices.

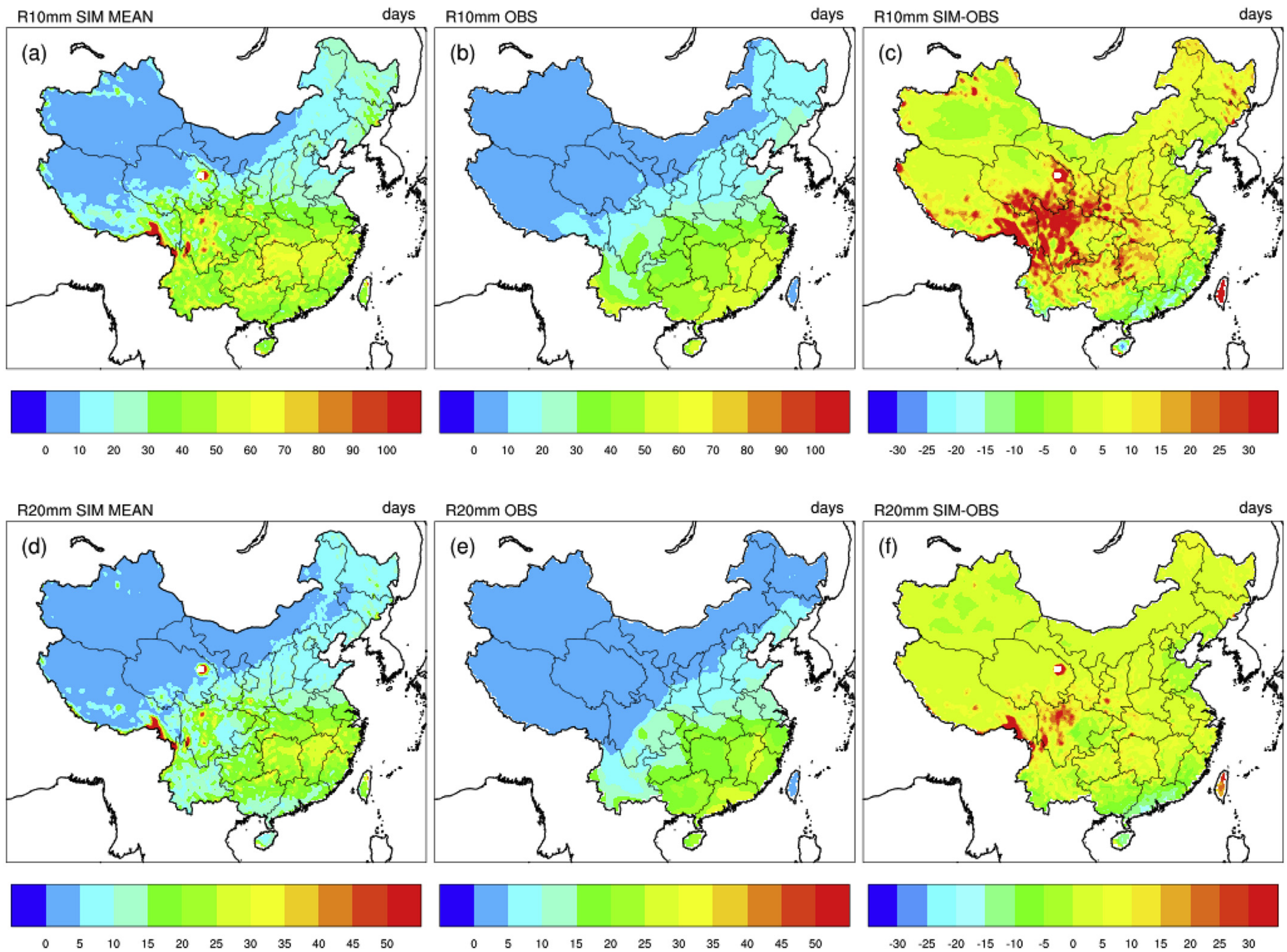

Fig. 8. Spatial comparisons (unit: days) between simulation and observation over China for the R10mm and R20mm during the baseline period (1961–1990). The simulated values are the average of six simulations ensemble (Q0, Q1, Q7, Q10, Q13 and ECHAM5).

3.1.2. Evaluation for inter-annual variability

As presented in Fig. 3, we apply the IVS skill score to quantify the ability of PRECIS in inter-annual variability between the ensemble models and observation. The performance for frequency indices is better than intensity indices in inter-annual variability, especially for CDD and R10mm. This is quite different from the Taylor diagram. For example, relative to poor performance in spatial variation for CDD, the IVS value is close to 0, and the value ranged from 0.5 to 0.8 for R10mm. Correspondingly, two intensity indices (Rx1day and R99pTOT) have the highest IVS values. Take R99pTOT for example, the IVS value is more than 1.8 for ECHAN5 model. Nevertheless, the overall IVS values simulated by PRECIS are less than some results from GCMs (Duan and Mei, 2014).

3.1.3. Calculation of rank and weight

Fig. 4 displays the ensemble models' rankings in terms of the Taylor diagram. Three evaluation indicators, including pattern correlation (left), spatial standardized deviation ratio (center), and root-mean square difference (right), are shown for each extreme index. The better ranking is shown in blue and the worse in red. Overall, the ranks of Q1, Q10 and Q13 are better than Q0, Q7and ECHAM5. According to the Table 1, the ranks of six simulations between Taylor diagram and IVS are similar, with a little difference in rank fourth and sixth. The results show the highest weight (0.411) is obtained by Q10 because of its top rank, followed by Q13 (0.205), Q1 (0.137), Q0 (0.082), Q7 (0.082), ECHAM5 (0.082).

3.1.4. Weighted validation in spatial distribution

The weighted annual average simulations using PRECIS ensemble are compared with observation in spatial distributions from 1961 to 1990 (As shown Figs. 5–9). Overall, the simulated distributions of all extreme indicators suggest that the PRECIS can reasonably reproduce the extreme temperature patterns in most regions of China, although there are some disagreements in some areas.

During the baseline period, the simulations for four precipitation intensity indices, maximum 1-day precipitation (Rx1day), maximum 5-day precipitation (Rx5day), very wet day precipitation (R95pTOT) and extremely wet day precipitation (R99pTOT), show similar spatial patterns with an increase from northwestern to southeastern China, though there are different biases in some sub-regions (Fig. 5). The northwest regions and southern edge show dry biases, particularly in the areas along Fujian and Guangdong, while prominent wet biases are conducted by RCMs in southwest regions (except for the east of Sichuan Basin). For example, the Rx5day overestimates over 30 mm in the south tip of Tibet and west of Sichuan. Rx1day depicts similar patterns as those of Rx5day, with a better performance over most regions of China. The R99pTOT resembles closely the maximum 5-day precipitation, implying that PRECIS could have some limitations in simulation on heavier extremely precipitation (Fig. 6).

For the frequency of extreme precipitation (Fig. 7), the maximum length of wet spell (CWD) is concentrated over the south and edge of Plateau and the biases between weighted multi-model ensemble mean and observation are maintained within in the range of [−10, 10] days

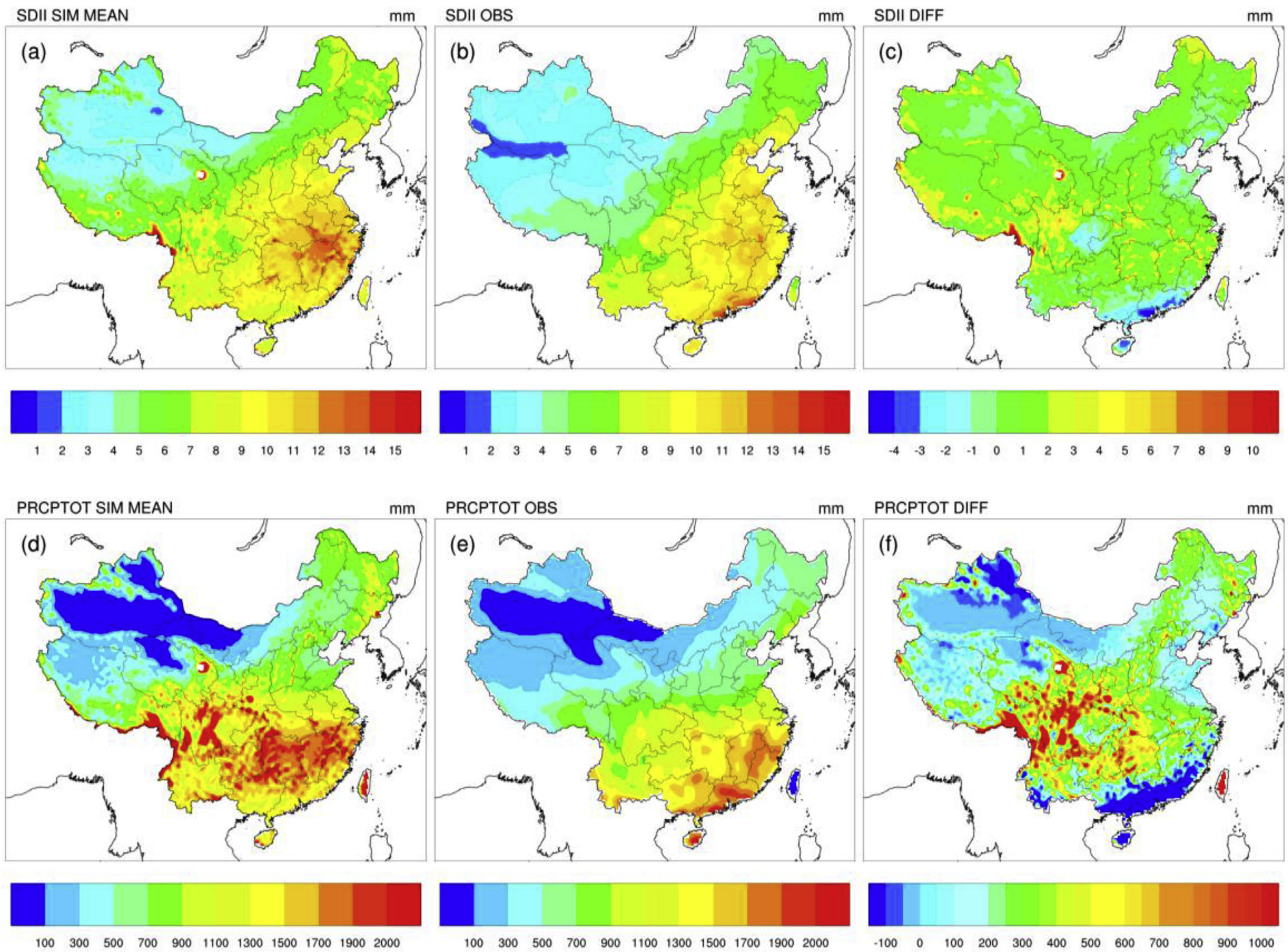

Fig. 9. Spatial comparisons between simulation and observation over China for the PRCPTOT (unit: mm) and SDII (unit: mm/day) during the baseline period (1961–1990). The simulated values are the average of six simulations ensemble (Q0, Q1, Q7, Q10, Q13 and ECHAM5).

for most regions of China. However, the maximum length of dry spell index (CDD) simulated by PRECIS has distinct differences in Xinjiang, where overestimation is in the north while underestimation is in the southern regions (Fig. 7c).

On the other hand, PRECIS can well simulate their spatial patterns of two fixed threshold-based indices, such as R10mm and R20mm (Fig. 8), and the simulated very heavy precipitation days (R20mm) are closer to the observed values than precipitation days (R10mm). Nevertheless, the simulated results tend to be somewhat lower along the southeast coast of China, while R10mm is overestimated in most southwestern regions.

Fig. 9 shows the simulations of simple precipitation intensity index (SDII) and annual total precipitation (PRCPTOT). Overall, SDII is slightly overestimated in most regions of China (about 1 mm/day) except for the southern Guangdong and Hainan. Simulated annual total precipitation exhibits apparent regional characteristics. There are large wet biases in the Midwest of China, but dry biases in southeast coast regions and the north of Xinjiang.

In general, PRECIS has the ability to reproduce ten precipitation extreme indices in spatial distribution in most regions of China during the baseline period, and shows better performance in eastern China. However, the simulations are overestimated in some parts of south and underestimated in the northwest and southern edge regions for most indices. The performance of PRECIS for frequency indices is better than that for intensity indices in inter-annual variability, especially for CDD and R10mm. But this is quite different in spatial variation from the Taylor diagram.

3.2. *Projection in changes*

3.2.1. *Changes in spatial distribution*

The projected absolute changes in spatial distribution for four precipitation extreme intensity indices in future three periods are shown in Fig. 10 for Rx1day and Rx5day, and Fig. 11 for R95pTOT and R99pTOT. The relative changes are shown in Figs. S1 and S2. An overall upward trend and greater extreme intensity in precipitation with time are observed. Relative to the reference period, the changes in the end of 21st century are greater than that in the begin of this century. The largest absolute changes occur in the southeast of China while weaker increasing amplitude is located in the northwest. For example, the absolute changes of Rx5day are projected to increase by 10 mm in Hunan but only by about 1 mm in southern Xinjiang in the end of this century (Fig. 10f). However, the relative changes exhibit an exactly inverse distribution. For example, the largest percentage changes appear mainly across southern Xinjiang and northern Qinghai while some southeastern regions show little changes. Because the overall rainfall is considerably scarce in arid and semi-arid regions, where little changes in precipitation would make very much difference. While in the southeast of China, there is rich rainfall so that the relative changes seem less remarkable albeit with larger absolute changes. Overall, the pattern of relative changes in Rx1day presents a general resemblance to that in Rx5day (Fig. S1), while in northwest regions, the relative increase in R95pTOT is larger than that in R99pTOT (Fig. S2).

For the R10mm and R20mm, we do not calculate the relative

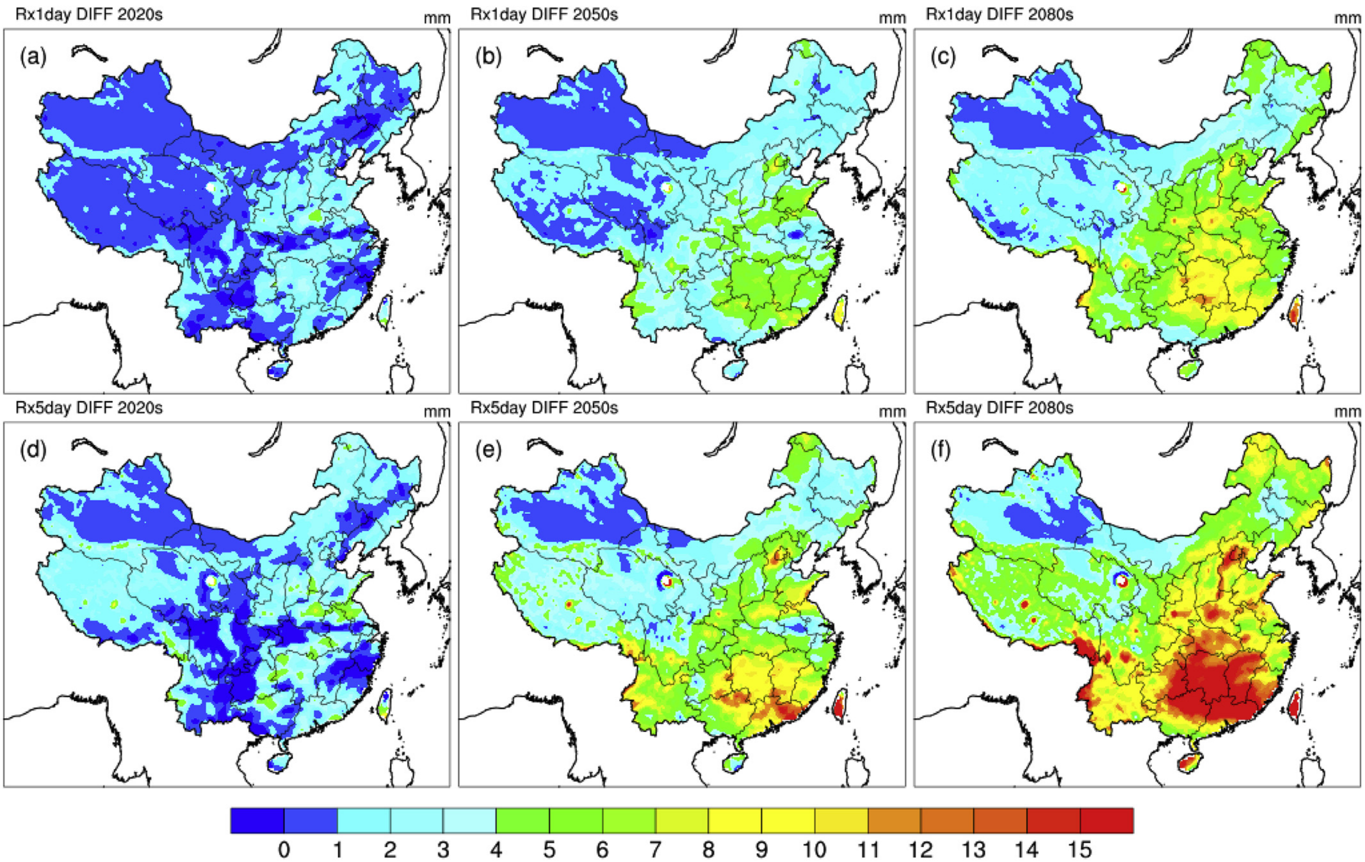

Fig. 10. Projected absolute changes (unit: mm) in spatial distribution for Rx1day and Rx5day. Columns from left to right are shown as 2020s, 2050s and 2080s, respectively.

changes owing to the seldom occurrences for heavy rain in some certain regions in the baseline period (i.e., Xinjiang). As shown in Fig. 12, decreases of heavy rain days (R10mm) in southwest, southeast and northeast are projected in the begin of this century. For example, R10mm would reduce 3 days approximately. Nevertheless, the entire region is projected to undergo consistent increase in R10mm and R20mm from 2050s. In the end of 21st century, the changes in number of heavy rain days are concentrated from Tibet to southern of China (Fig. 12c) and the very heavy rain days mainly increase in the southeast (Fig. 12f).

Fig. 13 and Figure S3 display the spatial changes of consecutive dry days (CDD) and consecutive wet days (CWD), with apparent incongruity compared with aforementioned indices. CDD is projected to decrease in most areas (except in southeast), for example, a decrease of 100 days or so occurs in the southern Xinjiang (Fig. 13a–c). In the other hand, the projected changes in CWD are increased in most regions of China (Fig. 13d–e) particularly in the eastern edge of the Tibetan Plateau (exceeding about 100 days). However, slightly decrease trend (about 10 days) is found in the southern end of Tibet and parts of southwest. In the view of percentage changes (Fig. S3), CDD tends to increase by 10% in southeast and CWD is inclined to increase by 50% in the northwestern and northern Tibet. The increasing CWD and decreasing CDD in northern China, especially in the southern Xinjiang, implying that there will be increasingly more wet days to alleviate regional drought in the future.

Overall, the annual total precipitation (PRCPTOT) is projected to increase continually in most regions of China in future, though decrease (−100 mm to −50 mm) appearing across parts of Sichuan, Yunnan and Fujian (Fig. 14a). The southern regions are expected to exhibit a larger increase in PRCPTOT than the north, even by 400 mm in the end of this century (Fig. 14c). The spatial distribution of relative change in PRCPTOT is generally similar to that in other indices, with larger values in the northwest of China. Simple precipitation intensity index (SDII), which is dependent on total annual precipitation and number of wet days, tends to apparently increase almost throughout the whole of China, particularly in the middle and end of 21st century, but slight decrease occurs in some scattered areas in northwest, which is likely due to the increase of local rain days (Figs. S4d–f).

3.2.2. Inter-annual changes

In the section, changes in precipitation extreme indices except the heavy and very heavy precipitation days (R10mm and R20mm) are expressed as percentage change relative to the reference period 1961–1990.

With respect to the baseline period, the trends of Rx1day and Rx5day tend to be approximately in the same way in future, with an increase by 2.44%/decade and 2.31%/decade, respectively (Fig. 15a–b). The rate of increase is larger in the first two periods of 21st century, especially in the middle. Take Rx1day for example, projected increasing trend is 2.92%/decade in the early, 5.08%/decade in the middle and 2.50%/decade in the end of 21st century, respectively. For other two intensity indices, the tendency for R95pTOT is almost the same as that for R99pTOT (Fig. 15c–d). Nevertheless, they show different growth rates in the middle of this century, with an increase of 6.00%/decade for R95pTOT and 8.34%/decade for R99pTOT. Moreover, R99pTOT presents much larger increasing magnitude, even exceeding 60% in some years.

Fig. 15e–h illustrates the temporal evolution of four frequency extreme indices. An increase is projected in CWD, R10mm and R20mm whereas decrease in CDD throughout 21st century. Specifically, CWD would increase by 10% by the end of this century with a rate of 0.21%/decade. On the contrary, CDD would decrease by about 9% and hold a

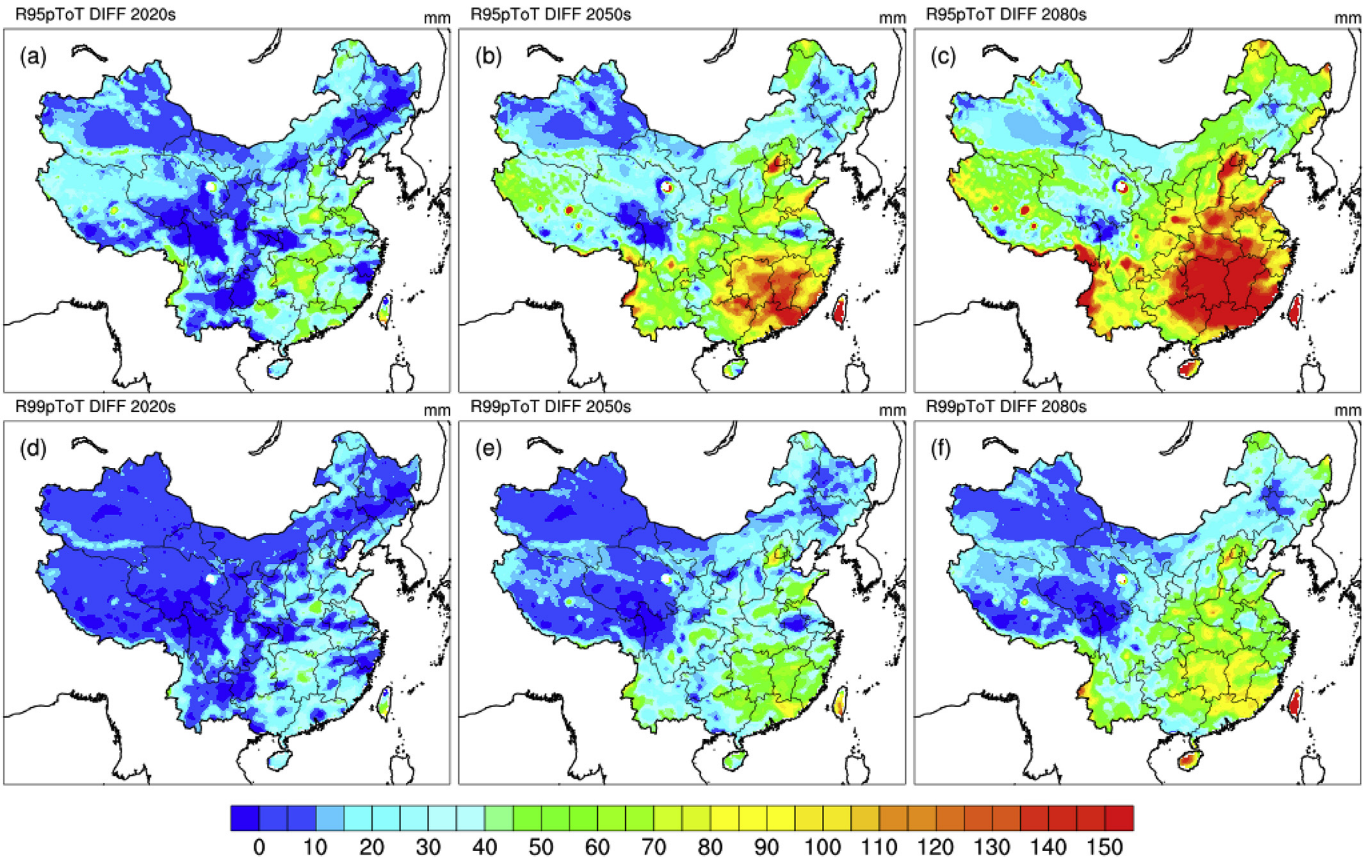

Fig. 11. Projected absolute changes (unit: mm) in spatial distribution for R95pTOT and R99pTOT. Columns from left to right are shown as 2020s, 2050s and 2080s, respectively.

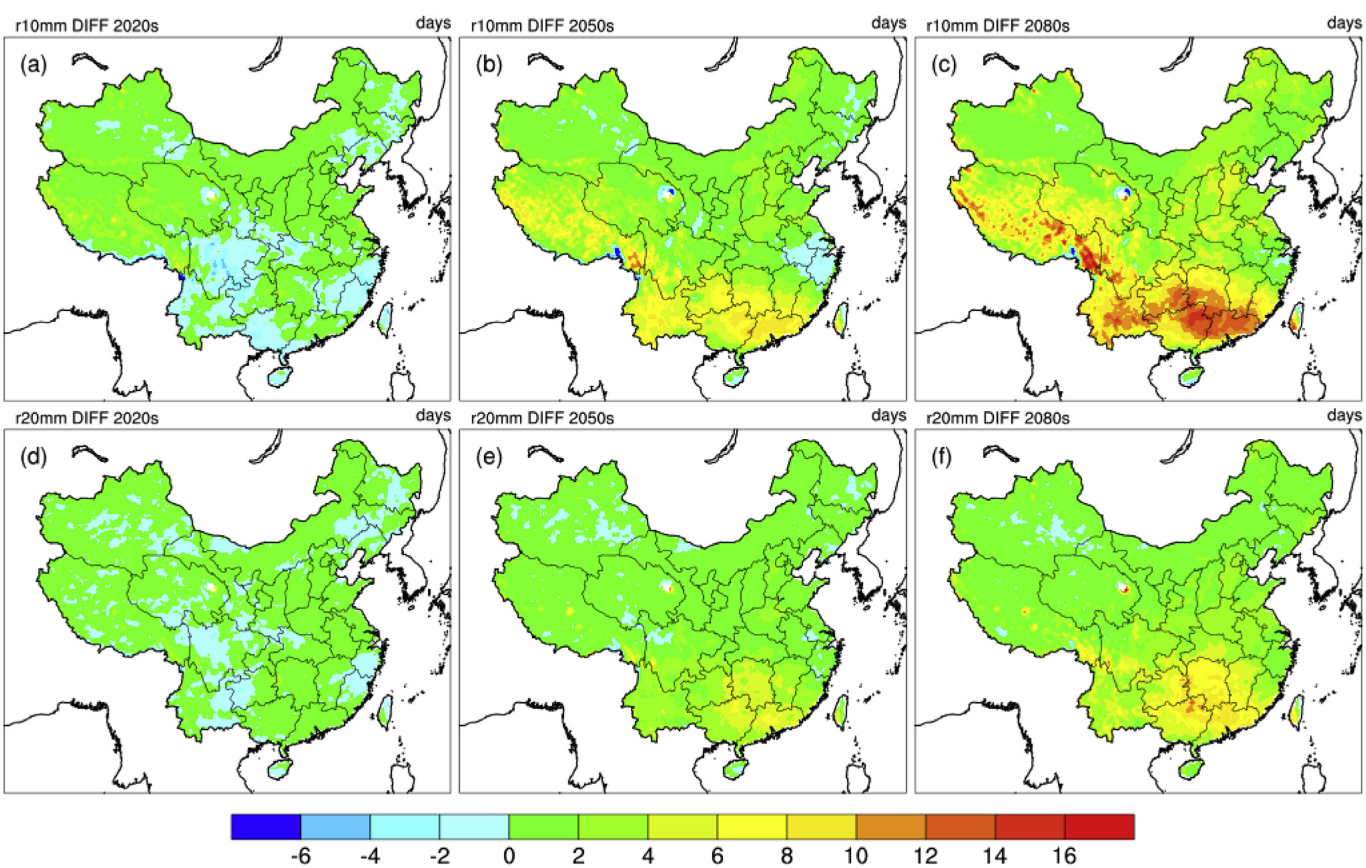

Fig. 12. Projected absolute changes (unit: days) in spatial distribution for R95pTOT and R99pTOT. Columns from left to right are shown as 2020s, 2050s and 2080s, respectively.

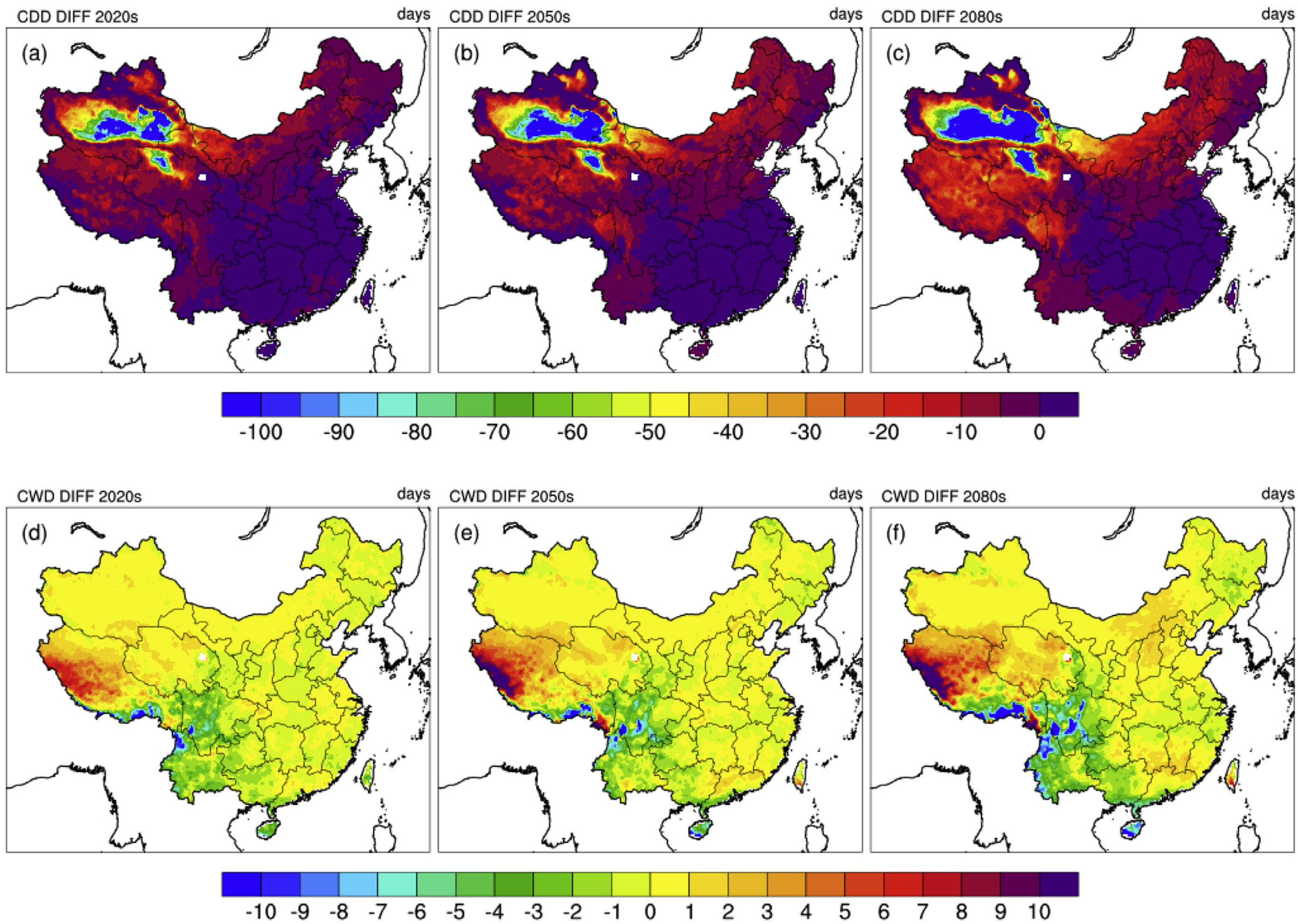

Fig. 13. Projected absolute changes (unit: days) in spatial distribution for CWD and CDD. Columns from left to right are shown as 2020s, 2050s and 2080s, respectively.

rate of 4.34%/decade especially in the middle of this century. Two indices of heavy precipitation days show consistent change, increasing by 4 days for R10mm and 2 days for R20mm by the end of century. The increase rate of R10mm (0.49%/decade) is projected to be slightly larger than R20mm (0.26%/decade).

The projected percentage changes in PRCPTOT and SDII are seen in Fig. 15i–j. The annual precipitation is likely to reach the peak in the middle of century, increasing by about 25% with a rate of 2.95%/decade, and from that, the trend begins to slightly decrease, with a rate of −0.12%/decade. By the end of century, SDII would increase about 15% with a rate of 1.43%/decade.

4. Discussions

4.1. Contribution of extreme precipitation

Generally speaking, the increases or decreases in precipitation extremes will affect the increase or decrease in annual total precipitation (Liu et al., 2013). Figs. S5–S6 show contribution rates of annual very wet day precipitation to annual total precipitation, number of heavy precipitation days to total wet days, respectively. The ratio to the enhancement of annual mean precipitation over China is about 50% in the early this century to 52% in the end of this century for R95pTOT and 21%–23% for R99pTOT. A slightly increase in the proportion of heavy rainfall to annual precipitation, with increasing trend at a rate of 0.14%/decade for R95pTOT and 0.12%/decade for R99pTOT. Moreover, the ratio between heavy rain days (R10mm and R20mm) and annual total wet days increment has consistent long-term positive trends, with a rate of 0.35%/decade for R10mm and 0.18%/decade for R20mm. The ratio to total wet days of R10mm is 18% in the early to 21% in the end of this century, and 6%–8% for R20mm. In summary, the ratio of heavy rainfall to total annual precipitation in both frequency and intensity will increase throughout 21st century, implying it may experience increasing floods over China in the future.

4.2. Potential physical attributions

Multiple interacting factors, including global warming, surface cover change, human actives, urbanization and the low-level cumulus cloud at regional scales, can affect the projection in future precipitation extremes (Wang et al., 2013). However, the remarkable warming temperature is the most important than the others. Many studies have demonstrated that the precipitation in China is highly sensitive to climate warming and the increasing temperature trends to trigger the magnitude and frequency of precipitation in China (Gu et al., 2017; Sun and Juan, 2013). According to the Clausius-Clapeyron equation, the atmospheric water vapor and precipitation will increase with approximately 7% per °C increase in temperature to the saturation concentrations (Ingram, 2016; Gu et al., 2017). It means that more water vapor will have better conditions to generate more precipitation. In this transition, the wetter storms will either become the wettest or more often, and ultimately result in the occurrence of heavy precipitation events more extreme or frequently.

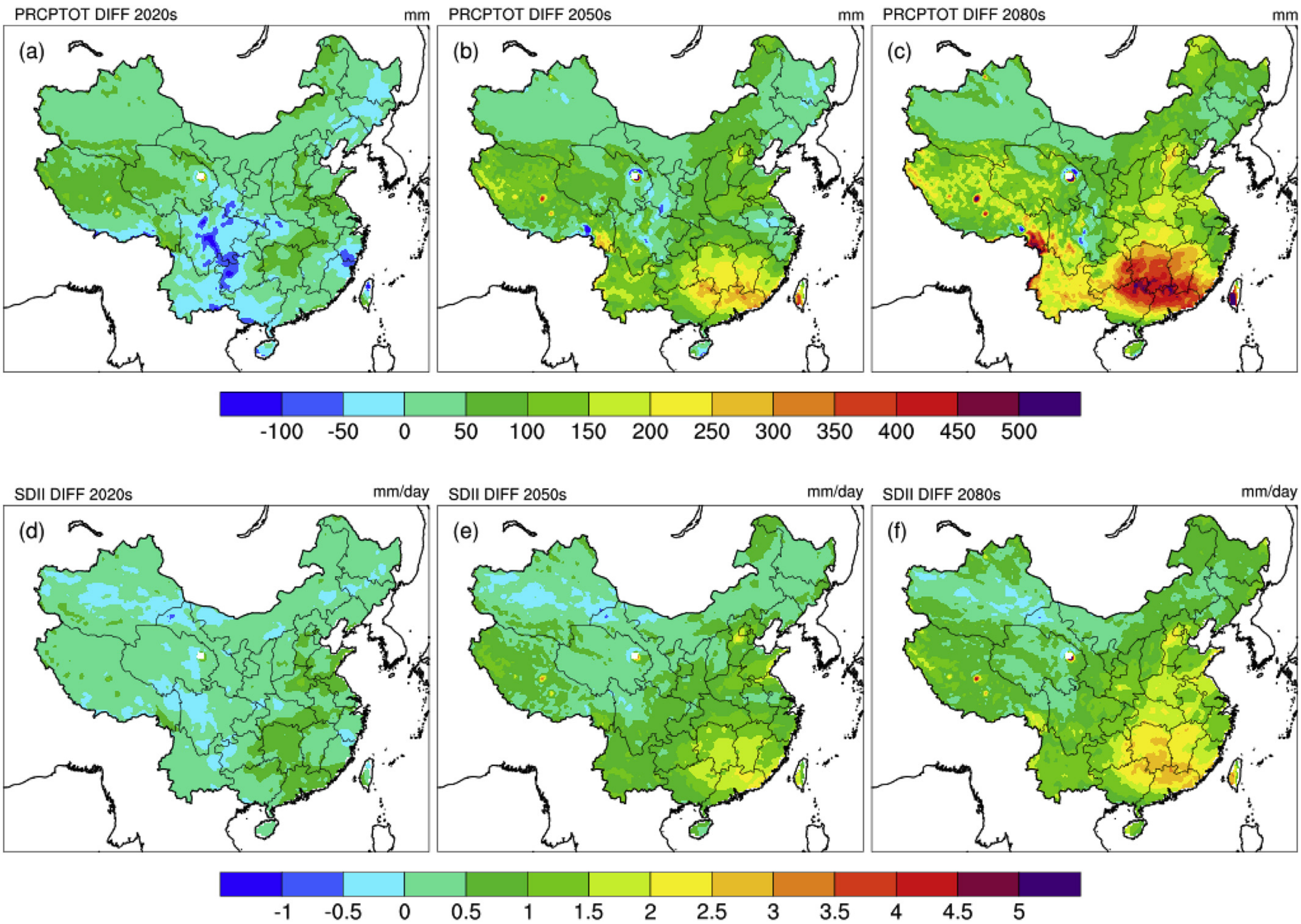

Fig. 14. Projected absolute changes in spatial distribution for PRCPTOT (unit: mm) and SDII (unit: mm/day). Columns from left to right are shown as 2020s, 2050s and 2080s, respectively.

On the other hand, the future potential changes in monsoon circulation also play a key role in the intensity and frequency of precipitation extremes over China. Some studies believe that the summer circulation will be stronger in East Asia, meaning that stronger southwesterly winds related to the North Pacific subtropical high will increase the inflow of warm and wet air from low latitudes directed toward the East Asia region. In addition, the northwesterly winds in winter formed by Siberian high pressure and Aleutian low pressure are considered more strengthened in future (Ying and Ding, 2010; Ham et al., 2016). The consequence of stronger circulations is an increase in evaporation and moist flux convergence, and further lead to increasing precipitation over the monsoon region (Seo and Ok, 2013).

In summary, the changes in thermal (i.e., temperature) and dynamical (i.e., circulations) factors could be some physical reasons for the increase of intensity and frequency in future precipitation over China.

5. Conclusions

In this study, potential changes in precipitation extreme (including ten indices) over China in response to global warming throughout the 21st century are projected through the PRECIS regional climate modeling system. A perturbed-physics ensemble from the UK Met Office HadCM3 and ECHAM5 are used to investigate the uncertainties caused by driving boundary conditions of PRECIS. The spatial resolution of the PRECIS ensemble simulations is 25 km with the purpose of reflecting the spatial variations of temperature extremes in the context of China.

During the baseline period (1961–1990), the simulated results are compared with the gridded climate dataset CN05.1, provided by the China Meteorological Administration. In general, PRECIS is able to reasonably reproduce the spatial patterns of current extreme precipitation over most regions of China for most indices, especially in the eastern China, though the simulations are overestimated in some parts of south and underestimated in the northwest and southern edge regions. The performance of PRECIS for frequency indices is better than that for intensity indices in inter-annual variability, especially for CDD and R10mm. But this is quite different in spatial variation from the Taylor diagram.

Future spatiotemporal changes of precipitation extreme indices as simulated by PRECIS in the 21st century are presented for three successive 30-year periods in this paper. Overall, the intensity indices, including Rx1day, Rx5day, R95pTOT, R99pTOT and SDII, are all projected to increase during the 21st century. The changes for frequency indices, including R10mm, R20mm and CWD, are similar to intensity indices. The CDD is projected to decrease during the 21st century. These conclusions are corresponding to other studies (Ji and Kang, 2015; Wang et al., 2012). The precipitation-related extreme indices indicate that it would likely experience more intensified and frequently extreme precipitation events, implying more risks of flooding on the whole of China in future. However, there is some regional diversity in the view of spatial distribution. The absolute changes are relatively small in north but large in southeast, while it is the opposite for relative changes. This means that precipitation extremes would have a far more positive impact in the north, especially in northwest in future. It would be likely greatly alleviate local drought problem and make this region

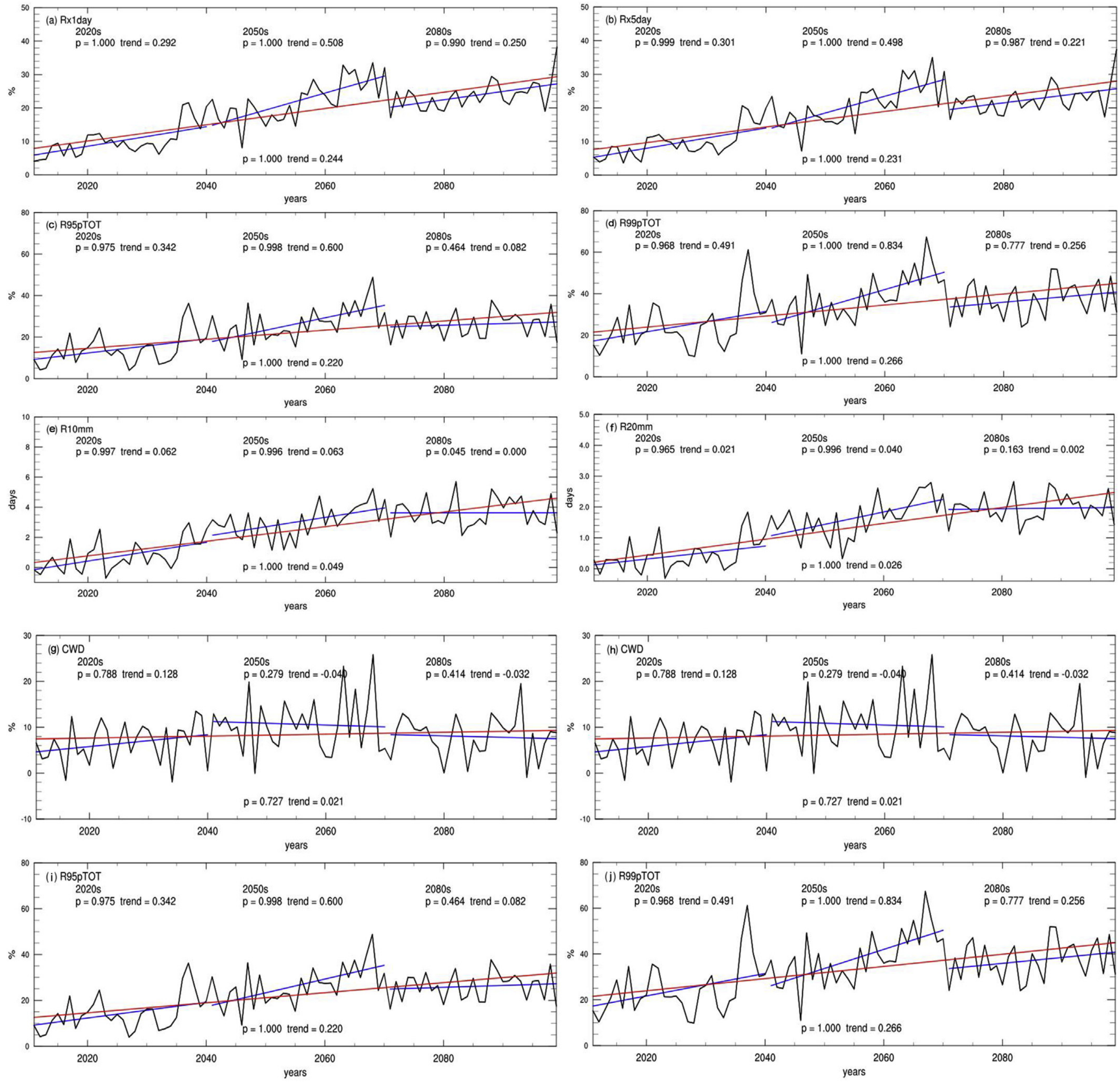

Fig. 15. Annual change in 10 precipitation indices averaged over the whole of China. All indices are calculated relative to 1961–1990. Colored lines show MK linear trends. The blue lines represent trends in future three periods and the red line represents the overall trend. (For interpretation of the references to color in this figure legend, the reader is referred to the Web version of this article.)

more suitable for rainfed agriculture. On the other hand, although there are little percentage changes in southeast, the total rainfall would increase remarkably beyond a reasonable doubt, suggesting there may be more flooding cases than in the past. Moreover, in the southwest regions, the decreasing CDD and CWD could signal an occurrence risk of both drought and flooding events, and people would face far bigger challenges in making adaptation strategies.

In the view of time evolution, except for CDD, all indices show an increase trend and the rate of increase is larger in the first two periods of 21st century, especially in the middle, demonstrating that the trends of precipitation-related indices are affected by future emission scenario. Moreover, the contributions of the annual very wet day precipitation to annual total precipitation and number of heavy precipitation days to total wet days are increasing with time. The ratio of very wet day precipitation (R95pTOT) to annual total precipitation increment over China is likely to exceed 50%, and the ratio in heavy rain days and annual total wet days may be 18% in the early to 21% in the end of this century for R10mm and 6%–8% for R20mm. The frequency and intensity of heavy rains across the country are projected to increase, implying that more frequent urban flooding would become a major challenge for developing resilient and sustainable communities in China. The changes in thermal (i.e., temperature) and dynamical (i.e., circulations) factors could be some physical reasons for the increase of intensity and frequency in future precipitation.

The ensemble results from our study can provide reliable and high-resolution climate projections for the entire country of China and can be used as direct inputs for climate change impact assessment and adaptation studies in order to help explore appropriate adaptation strategies against global climate change at regional and local scales.

Acknowledgments

This research was supported by the National Key Research and Development Plan (2016YFA0601502 and 2016YFE0102400), Fundamental Research Funds for the Central Universities (2017MS049), Environmental Protection Public Welfare Scientific Research Project (201509010).

Appendix A. Supplementary data

Supplementary data related to this article can be found at http://dx.doi.org/10.1016/j.atmosenv.2018.06.026.

References

Bell, J.L., Sloan, L.C., Snyder, M.A., 2004. Regional changes in extreme climatic events: a future climate scenario. J. Clim. 17, 81–87.
Bellprat, O., Kotlarski, S., L€uthi, D., Sch€ar, C., 2012. Exploring perturbed physics ensembles in a regional climate model. J. Clim. 25, 4582–4599.
Buontempo, C., Mathison, C., Jones, R., Williams, K., Wang, C., Mcsweeney, C., 2014. An ensemble climate projection for Africa. Clim. Dynam. 44, 1–22.
Chen, H.P., 2013. Projected change in extreme rainfall events in China by the end of the 21st century using CMIP5 models. Chin. Sci. Bull. 58, 1462–1472.
Chen, L., Frauenfeld, O.W., 2014. A comprehensive evaluation of precipitation simulations over China based on CMIP5 multimodel ensemble projections. Journal of Geophysical Research Atmospheres 119, 5767–5786.
Chen, H., Sun, J., 2015. Changes in climate extreme events in China associated with warming. Int. J. Climatol. 35, 2735–2751.
Collins, M., Booth, B.B.B., Harris, G.R., Murphy, J.M., Sexton, D.M.H., Webb, M.J., 2006. Towards quantifying uncertainty in transient climate change. Clim. Dynam. 27, 127–147.
Duan, K., Mei, Y., 2014. A comparison study of three statistical downscaling methods and their model-averaging ensemble for precipitation downscaling in China. Theor. Appl. Climatol. 116, 707–719.
Essery, R., Best, M., Cox, P.M., 2001. MOSES 2.2 technical documentation. Hadley Cent. Tech. Note 30, 1–31.
Fan, Y.R., Huang, W.W., Huang, G.H., Li, Y.P., Huang, K., Li, Z., 2016. Hydrologic risk analysis in the Yangtze River basin through coupling Gaussian mixtures into copulas. Adv. Water Resour. 88, 170–185.
Feng, L., Zhou, T., Wu, B., Li, T., Luo, J.J., 2011. Projection of future precipitation change over China with a high-resolution global atmospheric model. Adv. Atmos. Sci. 28, 464–476.
Fonseca, D., Carvalho, M.J., Marta-Almeida, M., Melo-Gonçalves, P., Rocha, A., 2016. Recent trends of extreme temperature indices for the Iberian Peninsula. Phys. Chem. Earth, Parts A/B/C 94, 66–76.
Gregory, D., Rowntree, P.R., 1990. A mass-flux convection scheme with representation of cloud ensemble characteristics and stability dependent closure. Mon. Weather Rev. 118, 1483–1506.
Gregory, D., Kershaw, R., Inness, P.M., 1997. Parametrization of momentum transport by convection II: tests in single column and general circulation models. Q. J. R. Meteorol. Soc. 123, 1153–1183.
Gu, X., Zhang, Q., Singh, V.P., et al., 2017. Changes in magnitude and frequency of heavy precipitation across China and its potential links to summer temperature. J. Hydrol. 547.
Guo, J., Huang, G., Wang, X., Li, Y., Lin, Q., 2017. Investigating future precipitation changes over China through a high-resolution regional climate model ensemble. Earths Future 5, 285–303.
Guo, J., Huang, G., Wang, X., Li, Y., Lin, Q., 2018. Dynamically-downscaled projections of changes in temperature extremes over China. Clim. Dynam. 50, 1045–1066.
Ham, S., Lee, J.W., Yoshimura, K., 2016. Assessing future climate changes in the east asian summer and winter monsoon using regional spectral mode. J. Meteorol. Soc. Jpn. Ser.ii 94, 69–87.
Hamed, K.H., Rao, A.R., 1998. A modified Mann-Kendall trend test for autocorrelated data. J. Hydrol. 204, 182–196.
Ingram, W., 2016. Extreme precipitation increases all round. Nat. Clim. Change 6, 443–444.
Ji, Z., Kang, S., 2015. Evaluation of extreme climate events using a regional climate model for China. Int. J. Climatol. 35, 888–902.
Jiang, Z., Li, W., Xu, J., Li, L., 2015. Extreme precipitation indices over China in CMIP5 models. Part I: model evaluation. J. Clim. 28 150902151739009.
Li, Z., He, Y., Wang, P., Theakstone, W.H., An, W., Wang, X., Lu, A., Zhang, W., Cao, W., 2012. Changes of daily climate extremes in southwestern China during 1961–2008. Global Planet. Change 80–81, 255–272.
Liu, W., Zhang, M., Wang, S., Wang, B., Li, F., Che, Y., 2013. Changes in precipitation extremes over Shaanxi Province, northwestern China, during 1960–2011. Quat. Int. 313–314, 118–129.
Lü, J.M., Ju, J.H., Ren, J.Z., Gan, W.W., 2012. The influence of the Madden-Julian Oscillation activity anomalies on Yunnan's extreme drought of 2009–2010. Sci. China Earth Sci. 55, 98–112.
Mcsweeney, C.F., Jones, R.G., Booth, B.B.B., 2012. Selecting ensemble members to provide regional climate change information. J. Clim. 25, 7100–7121.
Murphy, J.M., Sexton, D.M.H., Jenkins, G.J., Booth, B.B.B., Brown, C.C., Clark, R.T., Collins, M., Harris, G.R., Kendon, E.J., Betts, R.A., 2009. UK Climate Projections Science Report: Climate Change Projections. Uk Climate Projections Science Report Climate Change Projections. .
Noguer, M., Jones, R., Hassell, D., Hudson, D., Wilson, S., Jenkins, G., Mitchell, J., 2004. Workbook on Generating High Resolution Climate Change Scenarios Using PRECIS.
Pepler, A.S., Díaz, L.B., Prodhomme, C., Doblas-Reyes, F.J., Kumar, A., 2015. The ability of a multi-model seasonal forecasting ensemble to forecast the frequency of warm, cold and wet extremes. Weather & Clim. Extrem. 9, 68–77.
Qiu, J., 2010. China drought highlights future climate threats. Nature 465, 142–143.
Seo, K., Ok, J., 2013. Assessing future changes in the east asian summer monsoon using CMIP3 models: results from the best model ensemble. J. Clim. 26, 1807–1817.
Smith, R.N.B., 1990. A scheme for predicting layer clouds and their water content in a general circulation model. Q. J. R. Meteorol. Soc. 116, 435–460.
Stocker, T.F., Qin, D., Plattner, G.K., Alexander, L.V., Allen, S.K., Bindoff, N.L., Bréon, F.M., Church, J.A., Cubasch, U., Emori, S., 2013 IPCC, 2013. Technical summary. In: Stocker, T.F., Qin, D., Plattner, G.-K., Tignor, M., All, S.K. (Eds.), Climate Change 2013: the Physical Science Basis. Contribution of Working Group I to the Fifth Assessment Report of the Intergovernmental Panel on Climate Change, pp. 533–535.
Sun, JianQi, Juan, A.O., 2013. Changes in precipitation and extreme precipitation in a warming environment in China. Sci. Bull. 58 (12), 1395–1401.
Taylor, K.E., 2001. Summarizing multiple aspects of model performance in a single diagram. J. Geophys. Res. 106 (D7), 7183–7192 Journal of Geophysical Research Atmospheres. 106:7183-7192.
Wang, W., Chen, X., Shi, P., Phajmvan, G., 2008. Detecting changes in extreme precipitation and extreme streamflow in the Dongjiang River Basin in southern China. Hydrol. Earth Syst. Sci. 12, 207–221.
Wang, H.J., Sun, J.Q., Chen, H.P., Zhu, Y.L., Zhang, Y., Jiang, D.B., Lang, X.M., Fan, K., Yu, E.T., Yang, S., 2012. Extreme climate in China: facts, simulation and projection. Meteorol. Z. 21, 279–304.
Wang, B., Zhang, M., Wei, J., Wang, S., Li, S., Ma, Q., Li, X., Pan, S., 2013. Changes in extreme events of temperature and precipitation over Xinjiang, northwest China, during 1960–2009. Quat. Int. 298, 141–151.
Wang, F., Yang, S., Higgins, W., Li, Q., Zuo, Z., 2014a. Long-term changes in total and extreme precipitation over China and the United States and their links to oceanic–atmospheric features. Int. J. Climatol. 34, 286–302.
Wang, X., Huang, G., Liu, J., 2014b. Projected increases in intensity and frequency of rainfall extremes through a regional climate modeling approach †. J. Geophys. Res. Atmos. 119, 13.
Wang, X., Huang, G., Lin, Q., Nie, X., Liu, J., 2015a. High-resolution temperature and precipitation projections over Ontario, Canada: a coupled dynamical-statistical approach. Q. J. R. Meteorol. Soc. 141, 1137–1146.
Wang, X., Huang, G., Liu, J., Li, Z., Zhao, S., 2015b. Ensemble projections of regional climatic changes over ontario, Canada. J. Clim. 28, 7327–7346.
Wang, X., Huang, G., Baetz, B.W., 2016a. Dynamically-downscaled probabilistic projections of precipitation changes: a Canadian case study. Environ. Res. 148, 86–101.
Wang, X., Huang, G., Liu, J., 2016b. Twenty-first century probabilistic projections of precipitation over Ontario, Canada through a regional climate model ensemble. Clim. Dynam. 46, 3979–4001.
Wei, W., Shi, Z., Yang, X., Wei, Z., Liu, Y., Zhang, Z., Ge, G., Zhang, X., Guo, H., Zhang, K., 2017. Recent trends of extreme precipitation and their teleconnection with atmospheric circulation in the Beijing-tianjin sand source region, China, 1960–2014. Atmosphere 83.
Wu, J., Gao, X.J., 2013. A gridded daily observation dataset over China region and comparison with the other datasets. Chin. J. Geophys. 56, 1102–1111.
Wu, J., Gao, X., Giorgi, F., Chen, D., 2017. Changes of effective temperature and cold/hot days in late decades over China based on a high resolution gridded observation dataset. Int. J. Climatol. 37, 788–800.
Yin, H., Li, C., 2001. Human impact on floods and flood disasters on the Yangtze River. Geomorphology 41, 105–109.
Ying, S., Ding, Y.H., 2010. A projection of future changes in summer precipitation and monsoon in East Asia. Sci. China Earth Sci. 53 (2), 284–300.
Zhang, Y., Xu, Y., Dong, W., Cao, L., Sparrow, M., 2006. A future climate scenario of regional changes in extreme climate events over China using the PRECIS climate model. Geophys. Res. Lett. 33, 194–199.
Zhou, B., Wen, Q.H., Xu, Y., Song, L., Zhang, X., 2014. Projected changes in temperature and precipitation extremes in China by the CMIP5 multimodel ensembles. J. Clim. 27, 6591–6611.